

# Spatiotemporal variations of 100 m wind in Mongolia and implications for wind energy resources

Seong-Ho Hong<sup>1</sup> | Jambajamts Lkhamjav<sup>2</sup> | Han-Gyul Jin<sup>1</sup> | Jong-Jin Baik<sup>1</sup> 

<sup>1</sup>School of Earth and Environmental Sciences, Seoul National University, Seoul, South Korea

<sup>2</sup>Department of Applied Mathematics, National University of Mongolia, Ulaanbaatar, Mongolia

## Correspondence

Jong-Jin Baik, School of Earth and Environmental Sciences, Seoul National University, Seoul 08826, South Korea.  
Email: [jjaik@snu.ac.kr](mailto:jjaik@snu.ac.kr)

## Funding information

Chey Institute for Advanced Studies, National University of Mongolia, Grant/Award Number: NUM-P20193744

## Abstract

Mongolia is a high-altitude inland country, which experiences strong near-surface winds that could be valuable resources for wind power generation. In this study, we examine the spatiotemporal variations of 100 m wind and assess wind energy potential in Mongolia using the European Centre for Medium-Range Weather Forecasts Reanalysis version 5 (ERA5) data during 1979–2020. Mongolia exhibits two peaks in the monthly variation of 100 m wind, the higher peak in April and the lower peak in November. The eastern and southern (ES) region of the country is characterized by relatively high wind speed, night-time diurnal maximum of wind speed and relatively small amplitudes of monthly and diurnal variations of wind speed. This region is classified to have good potential for wind energy development with a long mean episode length. On the other hand, the western and northern (WN) region is characterized by relatively low wind speed, afternoon diurnal maximum of wind speed and relatively large amplitudes of monthly and diurnal variations of wind speed. This region is classified to have less wind energy potential. Four hotspots which have the greatest wind energy potential are found near the eastern border of Mongolia, south of the Gobi-Altai Mountains, near the southern border of Mongolia and in the southern region. Two principal modes of spatiotemporal variations of 100 m wind speed are obtained using the cyclostationary empirical orthogonal function (CSEOF) analysis method. The first CSEOF mode shows a spatial contrast between western and eastern Mongolia and is positively amplified in winter and negatively amplified in summer, which is associated with the seasonal change of the East Asian monsoon. The second mode is amplified in spring and autumn and shows mountain–basin contrasts that are reversed diurnally, which may be associated with the mountain–plains solenoid circulations and resultant vertical mixing of momentum.

## KEY WORDS

100 m wind, diurnal variation, Mongolia, seasonal variation, wind energy resources

## 1 | INTRODUCTION

Understanding the spatiotemporal variations of near-surface winds is of considerable importance in many

practical aspects such as air pollutant transport, wind hazard assessment, urban planning and wind energy resources. Many observational studies have been performed to characterize the spatial and/or temporal

variations of near-surface winds using surface observation and remote sensing data in different regions of the world. For instance, Yu et al. (2009) investigated the diurnal variation of surface wind in central eastern China using surface observation data and reported that the diurnal variation in this region is greatly influenced by geography-related factors such as the land-sea breezes and mountain-valley breezes. Abdou et al. (2010) examined the diurnal variation of lower boundary layer winds in the vicinity of Niamey, Niger under the influence of the West African monsoon using sodar measurements. The observed boundary layer wind profiles showed the night-time maximum at 200–400 m height and the morning maximum near the surface. Shu et al. (2020) used lidar measurements to examine the wind characteristics at an offshore platform near Hong Kong, China. They found that the monthly variation of wind speed shows its maximum in February and minimum in August and that the diurnal variation shows a daytime peak in summer and a night-time peak in autumn, which is associated with the land-sea thermal contrast that differs in the two seasons. The reported characteristics of near-surface winds are closely related to respective regional features, leading to distinct variations of near-surface winds in different regions.

Mongolia is a high-altitude inland country (1490 m, on average) with mountainous terrains in the western and northern parts, steppes in the eastern part and the Gobi Desert in the southeastern part. In winter, Mongolia is strongly affected by the Siberian High and thereby exhibits clear skies and stable atmosphere. In Mongolia, the lowest monthly mean air temperature appears in January, which ranges from  $-34$  to  $-30^{\circ}\text{C}$  in the high mountains, from  $-25$  to  $-20^{\circ}\text{C}$  in the steppes and from  $-15$  to  $-12^{\circ}\text{C}$  in the southern part of the Gobi Desert (Yembuu, 2020). In summer, subtropical air masses with continental origin come from the south and low-pressure systems control the climate in Mongolia. The highest monthly mean air temperature appears in July, ranging from  $5$  to  $15^{\circ}\text{C}$  in the mountains and from  $20$  to  $25^{\circ}\text{C}$  in the Gobi Desert and the southern part of the steppes (Yembuu, 2020). Mongolia also exhibits frequent occurrences of cyclogenesis, which maximize in spring (Zhang et al., 2012). Mongolia is one of the land regions that exhibit the strongest wind in East Asia, along with Inner Mongolia and the Tibetan Plateau (Yu et al., 2016). The strong wind in Mongolia is potentially valuable for electric power supplies through wind energy development (Chen et al., 2016). Also, it may induce occurrences of dust storms (Natsagdorj et al., 2003), which can cause yellow sand phenomena in East Asia (Takemi & Seino, 2005). These encourage the investigation of the near-surface wind climate in Mongolia.

Elliott et al. (2001) compiled multiple datasets for wind such as the observation data at meteorological stations, the wind profile data from radiosonde observations and the reanalysis data produced by the National Centers for Environmental Prediction (NCEP) and the National Center for Atmospheric Research (NCAR) with a resolution of  $\sim 210$  km and a temporal resolution of 6 h (Kalnay et al., 1996) to assess wind energy resources at 30 m above ground level in Mongolia. They reported that the eastern and central Mongolia have a larger amount of wind energy resources than western Mongolia. They also reported that the sites at low altitudes mostly exhibit April–May peaks of wind speed while the sites on ridge crests in western Mongolia exhibit October–December peaks. Yu et al. (2016) examined the seasonal and interannual variations of 80 m wind in East and South Asia using the Climate Forecast System Reanalysis (CFSR) data (Saha et al., 2010) produced by NCEP, which has a horizontal resolution of  $\sim 38$  km and a temporal resolution of 6 h. They found that the wind speed in southern Mongolia has decreased during 1979–2011 and attributed it to the increase of sea-level pressure in Mongolia.

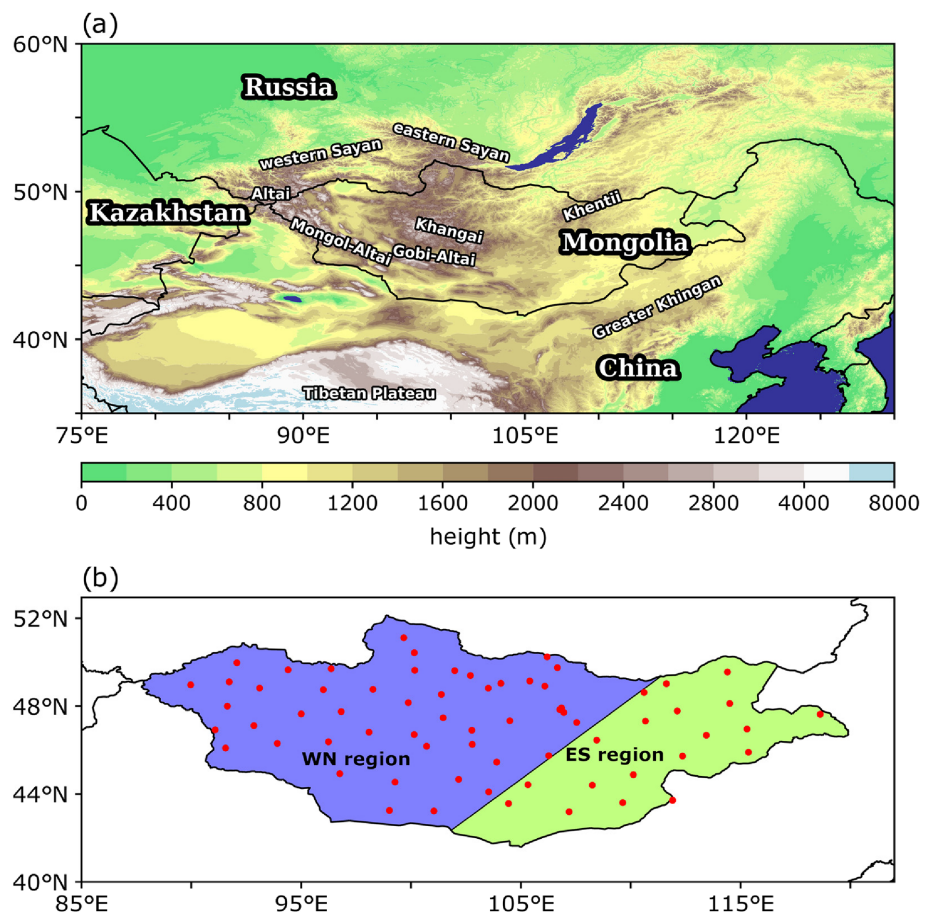
Given that the typical hub height of wind turbines has increased from about 30 m to about 80–130 m during the past two decades (Lantz et al., 2019), the characterization of the wind climate at the hub height of modern wind turbines is needed. The objectives of this study are to examine the spatiotemporal variations of 100 m wind and their possible mechanisms and to assess wind energy potential in Mongolia. We focus especially on the diurnal variation, because knowing the diurnal differences between the electricity production and electricity demand is important for the planning of wind power generation (e.g., Mulder, 2014). In addition, we use modern reanalysis data with finer temporal (1 h) and spatial ( $\sim 30$  km) resolutions than those of the reanalysis data used in the previous studies, to identify detailed characteristics of diurnal and regional variations of wind. The rest of this paper is arranged as follows: In section 2, data and methods are described. In section 3, the reanalysis dataset for wind used in this study is validated. In section 4, the results are presented and discussed. In section 5, a summary and conclusions are provided.

## 2 | DATA AND METHODS

### 2.1 | Data

To examine the spatiotemporal variations of wind and their mechanisms, the 100 m zonal and meridional components of wind, surface pressure, 2 m temperature, 700 hPa geopotential height and 700 hPa zonal and

**FIGURE 1** (a) Topographic map of Mongolia and surrounding regions. (b) Locations of 67 surface wind observation stations (red circles) in Mongolia. The eastern and southern region (ES region) and the western and northern region (WN region) are shaded by yellow-green and blue colours, respectively, in (b) [Colour figure can be viewed at [wileyonlinelibrary.com](http://wileyonlinelibrary.com)]



meridional components of wind data during 42 years (1979–2020) from the European Centre for Medium-Range Weather Forecasts Reanalysis version 5 (ERA5; Hersbach et al., 2020) with a temporal resolution of 1 h and a horizontal resolution of  $0.25^\circ \times 0.25^\circ$  are used. The ERA5 data have been reported to have higher reliability for near-surface wind speeds than other reanalysis data (Olauson, 2018; Ramon et al., 2019) and have been used for the assessments of wind energy resources or wind characteristics (Boudia & Santos, 2019; Gubbala et al., 2021; Nezhad et al., 2021; Pryor & Barthelmie, 2021). Although the 100 m wind is the variable of interest in this study, the 100 m wind in the ERA5 data cannot be directly evaluated because the observation data of 100 m wind in Mongolia are not available. For this reason, the 10 m wind in the ERA5 data is additionally used to evaluate the reliability of the 100 m wind data indirectly. In ERA5 in which the observation of 10 m wind over land are not assimilated, the 10 m and 100 m winds over land are diagnostically estimated from winds at the model levels close to the surface. The 10 m wind is estimated using wind at the blending height (40 m or the lowest model level) and the Monin-Obukhov similarity theory (ECMWF, 2021). The 100 m wind is estimated by the linear

interpolation using the winds at the two model levels adjacent to 100 m.

For the evaluation, 3-hourly 10 m wind observation data during the same period at 67 stations of the National Agency for Meteorology and Environment Monitoring of Mongolia are used (Figure 1b). The station elevation ranges from 628 to 2257 m above the mean sea level. The observation data are quality-controlled by excluding the data of which wind speed exceeds the upper limit of the reliable measurement for the instruments. At all stations, the number of missing data does not exceed 3% of the total.

## 2.2 | Wind classes and wind energy metrics

To assess 100 m wind energy resources in Mongolia, first we calculate the wind power density (WPD) as follows:

$$WPD = \frac{1}{2} \rho V^3, \quad (1)$$

where  $\rho$  is the air density and  $V$  is the 100 m horizontal wind speed. Here,  $\rho$  is calculated from surface pressure

Resource potential			
Class	Rural	Utility	Wind power density (WPD; $\text{W}\cdot\text{m}^{-2}$ )
1	Moderate	Marginal	$100 \leq \text{WPD} < 200$
2	Good	Moderate	$200 \leq \text{WPD} < 300$
3	Excellent	Good	$300 \leq \text{WPD} < 400$
4	Excellent	Excellent	$400 \leq \text{WPD}$

TABLE 1 Wind resource potential according to the classification of wind power density

and 2 m temperature in the ERA5 data. Note that WPD is calculated for every hour. Then, we calculate the mean WPD and classify it into four classes, similar to the classification of Elliott et al. (2001). The classification is presented in Table 1. In Mongolia, a third of its population engages in primary industries (e.g., agriculture and animal husbandry) and has a nomadic lifestyle (Chen et al., 2016). Accordingly, the assessment of wind energy resources for rural (i.e., village power and nomadic) application is just as important as that for utility application. The classification of Elliott et al. (2001) offers the assessment of wind energy resources for both the types of electric use. Although Elliott et al. (2001) considered the hub height of 30 m instead of 100 m used in this study, the classification thresholds of wind energy resources are not modified in this study because they were determined by considering the suitability of the absolute amount of wind power density, regardless of the hub height.

In addition to the wind classes, two metrics (Ren et al., 2019) are used to assess wind energy potential in Mongolia. They are the mean episode length and mean lull. The mean episode length (mean lull) is defined as the mean length of consecutive hours with wind power density higher (lower) than a threshold wind power density. The longer mean episode length (mean lull) indicates that the wind power density higher (lower) than the threshold wind power density is maintained for a longer time. Here, the threshold wind power density is set as  $300 \text{ W}\cdot\text{m}^{-2}$ , above which the wind power density is good for utility application and excellent for rural application (Table 1). These two quantities give information about the intermittency of sufficient and insufficient wind energy resources.

### 2.3 | CSEOF analysis method

The cyclostationary empirical orthogonal function (CSEOF) analysis method is performed to characterize the spatiotemporal variations of 100 m wind in Mongolia and to examine the associated mechanisms. The CSEOF analysis can be useful to identify distinct spatiotemporal variation modes of a variable (Kim, 2017). Here, we

briefly describe the CSEOF analysis method, which can facilitate the interpretation of the analysis results. Detailed descriptions of the analysis method are given in Kim and North (1997) and Kim (2017).

The data of a variable  $T(r, t)$  are decomposed into multiple modes of the periodic spatiotemporal pattern  $B_n(r, t)$  with the period  $d$  and the corresponding time-varying amplitudes  $T_n(t)$ ,

$$T(r, t) = \sum_n B_n(r, t) T_n(t), \quad (2)$$

$$B_n(r, t) = B_n(r, t+d), \quad (3)$$

where  $r$  and  $t$  are the spatial and temporal points, respectively, and  $n$  is the mode number. Here,  $B_n(r, t)$  is called the CSEOF loading vector (CSLV) and  $T_n(t)$  is called the principal component (PC) time series. In this study, 24 h is chosen as the period  $d$ . The CSLVs are mutually orthogonal to each other, and the PC time series are mutually uncorrelated to each other,

$$\frac{1}{Nd} \sum_{r=1}^N \sum_{t=1}^d B_n(r, t) B_m(r, t) = \delta_{nm}, \quad (4)$$

$$\frac{1}{M} \sum_{t=1}^M T_n(t) T_m(t) = \lambda_n \delta_{nm}, \quad (5)$$

where  $N$  and  $M$  are the numbers of spatial and temporal points in the data, respectively,  $\delta_{nm}$  is the Kronecker delta and  $\lambda_n$  is the variance of  $T_n(t)$ . It is considered that each mode corresponds to a distinct physical process.

After the distinct modes of  $T(r, t)$  are identified, the regression analysis is conducted for other meteorological variables to examine the mechanisms that are related to each mode of  $T(r, t)$ . The regression analysis on another variable  $P(r, t)$  gives the spatiotemporal variation of  $P(r, t)$  that is related to each CSEOF mode of  $T(r, t)$ . In this analysis,  $P(r, t)$  is called the predictor variable and  $T(r, t)$  is called the target variable. For this,  $P(r, t)$  is decomposed into multiple modes, each of which has a PC time series that is identical to that of  $T(r, t)$ , that is,  $T_n(t)$ ,

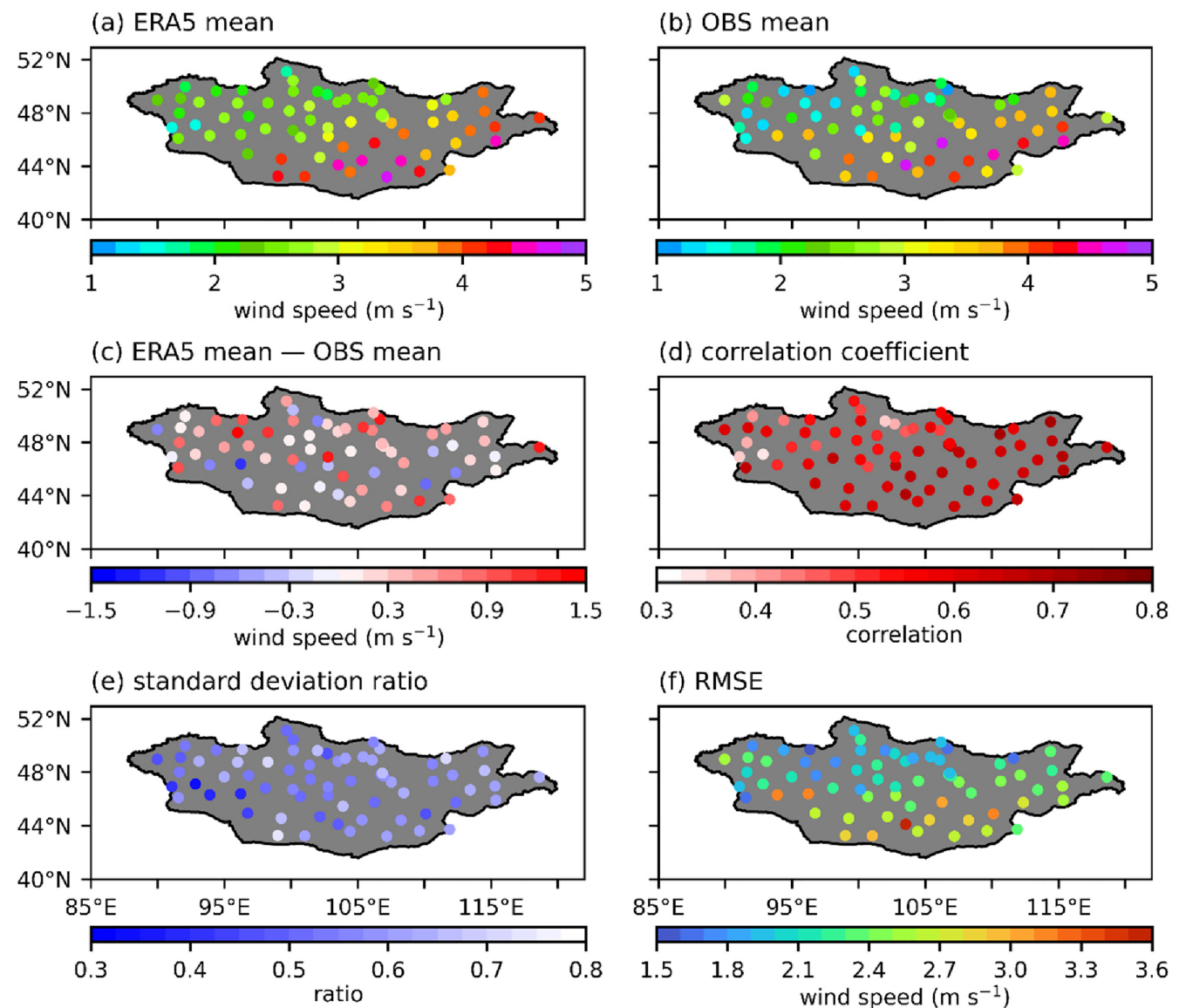


**FIGURE 2** Spatial distributions of 10 m wind speed averaged over the period 1979–2020 for the (a) ERA5 data, (b) observation and (c) their difference. Spatial distributions of (d) correlation coefficient, (e) standard deviation ratio and (f) root-mean-square error (RMSE) between the observation and ERA5 data. The standard deviation ratio is calculated as the standard deviation of 10 m wind speed in the ERA5 data divided by that in the observation [Colour figure can be viewed at [wileyonlinelibrary.com](http://wileyonlinelibrary.com)]

$$P(r, t) = \sum_n C_n^{(\text{reg})}(r, t) T_n(t), \quad (6)$$

where  $C_n^{(\text{reg})}(r, t)$  is the periodic spatiotemporal pattern extracted from  $P(r, t)$ . Each  $C_n^{(\text{reg})}(r, t)$  is considered to be physically consistent with the corresponding  $B_n(r, t)$ . The regression analysis method can be a useful tool to examine the physical mechanism responsible for each CSEOF mode of the target variable. In this study, the target variable is the anomaly of 100 m wind speed. As the predictor variables, the anomalies of 100 m zonal and meridional components of wind, 700 hPa geopotential height and

700 hPa zonal and meridional components of wind are selected. The reason for regressing the anomalies of zonal and meridional components of 100 m wind to the 100 m wind speed anomaly is to gain physical consistency between each CSEOF modes of the wind speed and wind vector. The 700 hPa level is selected because generally in Mongolia, this level is the closest pressure level to the 100 m height among the mandatory pressure levels that are not under direct influence of the surface. The anomaly of a variable is calculated by subtracting its temporal mean. Then, the 42-year anomaly data are averaged over years to produce 1-year-length mean data.

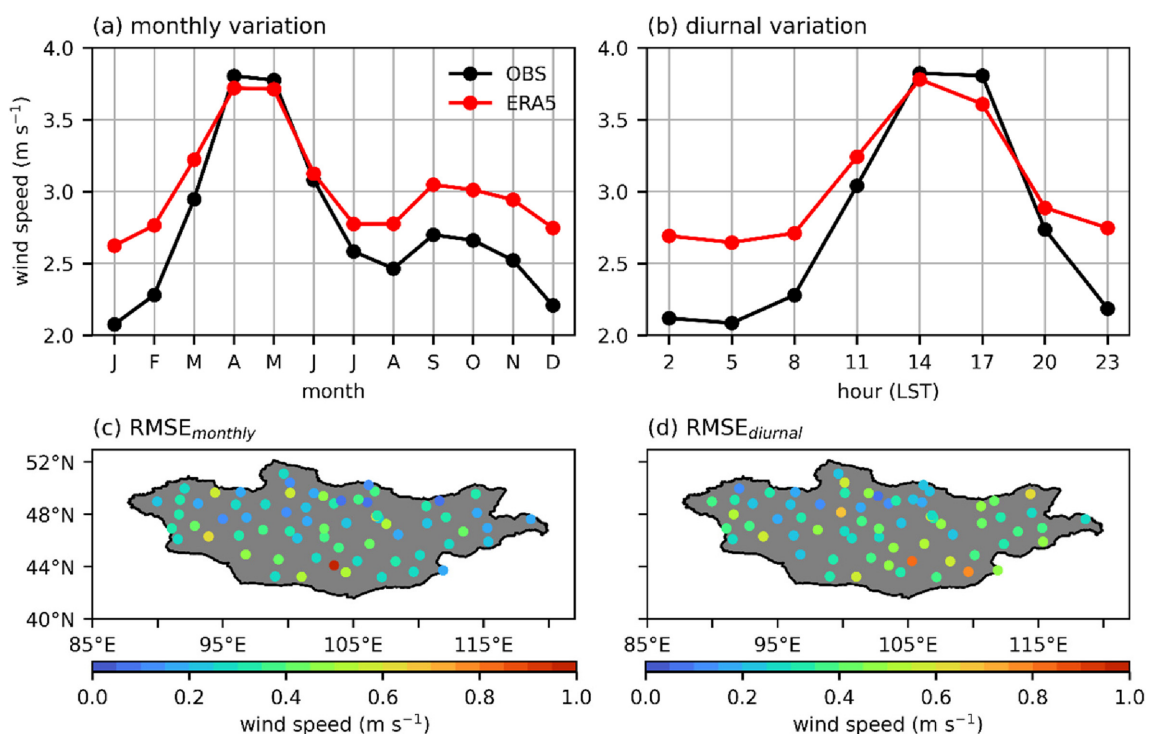


**FIGURE 3** (a) Monthly and (b) diurnal variations of 10 m wind speed averaged over the locations of 67 stations and the period 1979–2020 for the observation (black) and ERA5 data (red). Note that the ERA5 data are bilinearly interpolated to the locations of the observation stations. Spatial distributions of RMSE for the 42-year averaged (c) monthly and (d) diurnal variations [Colour figure can be viewed at [wileyonlinelibrary.com](http://wileyonlinelibrary.com)]

### 3 | VALIDATION OF ERA5 NEAR-SURFACE WIND

In this section, the ERA5 10 m wind speed data are compared with the 10 m wind speed observation for the evaluation of near-surface wind speed in the ERA5 data. For comparison, the ERA5 data are bilinearly interpolated to the locations of the observation stations. The spatial distributions of mean 10 m wind speed for the observation and ERA5 data and their difference as well as the spatial distributions of correlation coefficient, standard deviation ratio and root-mean-square error (RMSE) between the observation and ERA5 data are presented in Figure 2. The overall spatial pattern of the mean wind speed in the ERA5 data (Figure 2a) is similar to that in the observation (Figure 2b). The ERA5 data show low wind speed in western and northern Mongolia (see Figure 1a) and show high wind speed in eastern and southern Mongolia, which generally agrees with the observation. The ERA5 data overestimate wind speed for 75% of stations (Figure 2c). The overestimation or underestimation of wind speed is slightly larger in western and northern Mongolia with complex topography compared to eastern and southern Mongolia with much less complex topography, which is shown by the larger mean absolute bias in

the former regions ( $0.52 \text{ m s}^{-1}$ ) than in the latter regions ( $0.48 \text{ m s}^{-1}$ ). The correlation between the observation and ERA5 data is generally strong except at the stations near the Altai Mountains and eastern Sayan Mountains (Figure 2d). The standard deviation ratio is smaller than 1 for all stations (Figure 2e), which indicates that the ERA5 data underestimate the amplitude of temporal variation of wind speed. Some mountainous regions such as the Mongol-Altai Mountains (see Figure 1a) show relatively small standard deviation ratios. The RMSE between the observation and ERA data ranges from 1.5 to  $3.7 \text{ m s}^{-1}$  across the stations (Figure 2f).

Figure 3 shows the monthly and diurnal variations of 10 m wind speed for the observation and ERA5 data and the spatial distributions of RMSE for the 42-year averaged monthly and diurnal variations. In the monthly variation (Figure 3a), the ERA5 data show a bimodal pattern with a peak in April and the other peak in September, which agrees with the observation. Also, the ERA5 data and observation both show the lowest monthly mean wind speed in January. However, the ERA5 data slightly underestimate the monthly mean wind speed in April and May and overestimate it for the rest of the year. The overestimation is most prominent in December and January. The amplitude of the monthly variation is

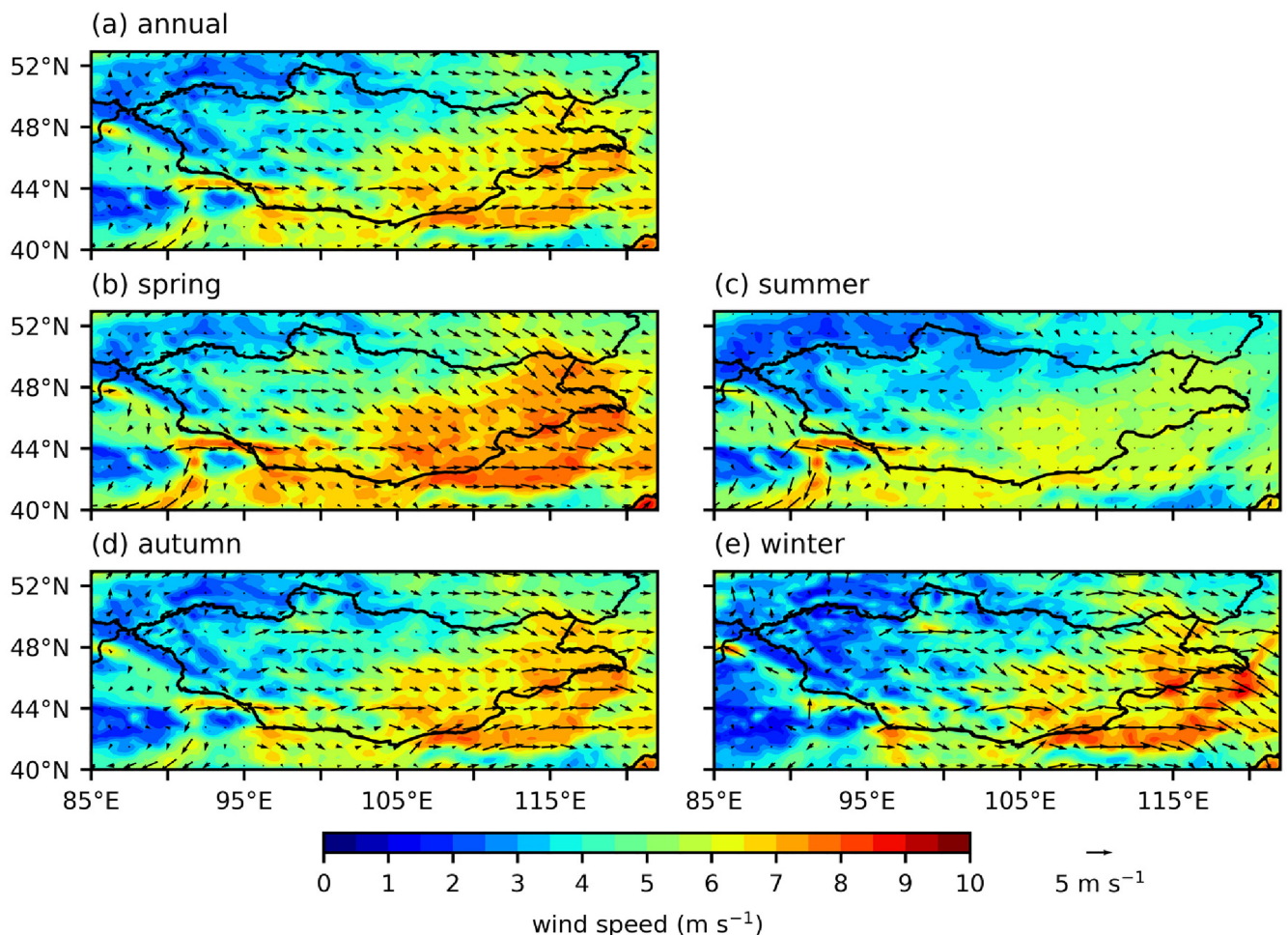


**FIGURE 4** Spatial distributions of 100 m wind speed (shades) and wind vector (arrows) averaged over the period 1979–2020 for (a) the whole year, (b) spring, (c) summer, (d) autumn and (e) winter [Colour figure can be viewed at [wileyonlinelibrary.com](http://wileyonlinelibrary.com)]

underestimated in the ERA5 data. Unlike the RMSE calculated using individual data (Figure 2f), the RMSE for the monthly variation is smaller than  $0.5 \text{ m}\cdot\text{s}^{-1}$  at 59 out of 67 stations (Figure 3c), which indicates that the ERA5 data can reliably reproduce the climatological monthly variation of wind speed. In the diurnal variation (Figure 3b), both the observation and ERA5 data show high wind speed in the afternoon with a maximum at 1400 LST (UTC + 8 h) and low wind speed in the nighttime with a minimum at 0500 LST. The ERA5 data slightly underestimate wind speed at 1400 and 1700 LST and overestimate it for the rest of the day. As in the monthly variation, the amplitude of the diurnal variation is underestimated in the ERA5 data. The RMSE for the diurnal variation (Figure 3d) is smaller than  $0.5 \text{ m}\cdot\text{s}^{-1}$  at 56 out of 67 stations, indicating that the ERA5 data well capture the climatological diurnal variation of wind speed.

The above results from Figures 2 and 3 suggest that the ERA5 data well reproduce the climatological seasonal

and diurnal variations of 10 m wind speed with some underestimations of the amplitude of the variations. This allows us to use the ERA5 data for studying seasonal and diurnal variations of wind speed in Mongolia.

## 4 | RESULTS AND DISCUSSION

### 4.1 | Spatiotemporal variations of 100 m wind

#### 4.1.1 | Seasonal variation

Figure 4 shows the spatial distributions of annual and seasonal mean 100 m wind speed and wind vector. Here, the mean wind speed is calculated by averaging the wind speed itself and the mean wind vector is calculated by averaging each component of the wind vector separately. The annual mean wind speed is higher in eastern and southern Mongolia ( $6.4 \text{ m}\cdot\text{s}^{-1}$ ) than in western and

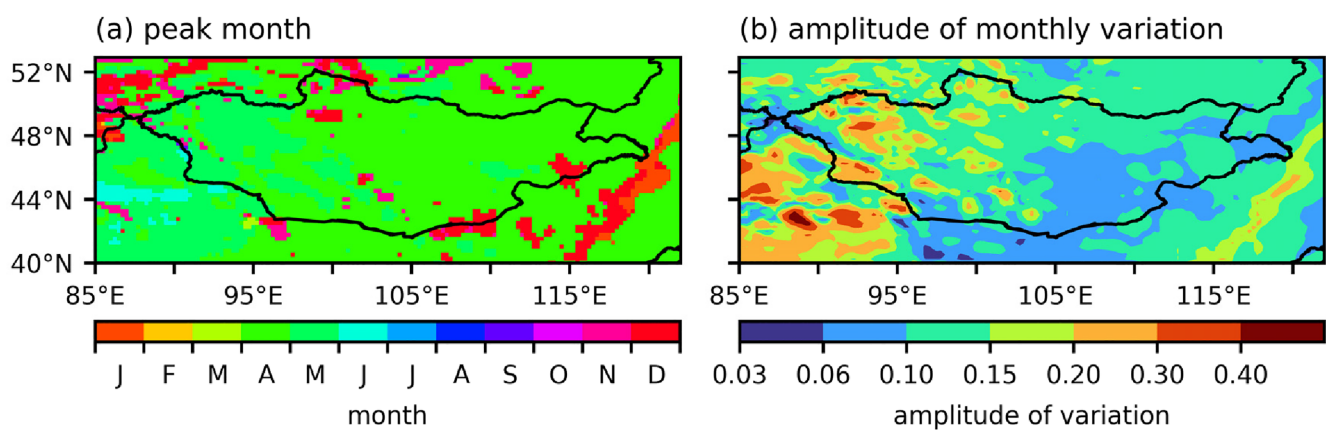


**FIGURE 5** Spatial distributions of (a) peak month and (b) amplitude of monthly variation for 100 m wind speed averaged over the period 1979–2020 [Colour figure can be viewed at [wileyonlinelibrary.com](http://wileyonlinelibrary.com)]

northern Mongolia ( $4.2 \text{ m}\cdot\text{s}^{-1}$ ) (Figure 4a), as in 10 m. The four hotspots of wind speed are found near the eastern border of Mongolia ( $\sim 114^\circ\text{--}116^\circ\text{E}$ ,  $\sim 45^\circ\text{--}47^\circ\text{N}$ ;  $7.7 \text{ m}\cdot\text{s}^{-1}$ ), south of the Gobi-Altai Mountains ( $\sim 96^\circ\text{--}98^\circ\text{E}$ ,  $\sim 43^\circ\text{--}45^\circ\text{N}$ ;  $7.7 \text{ m}\cdot\text{s}^{-1}$ ), near the southern border of Mongolia ( $\sim 107^\circ\text{--}109^\circ\text{E}$ ,  $\sim 42^\circ\text{--}44^\circ\text{N}$ ;  $7.6 \text{ m}\cdot\text{s}^{-1}$ ) and in the southern region ( $\sim 105^\circ\text{--}108^\circ\text{E}$ ,  $\sim 43^\circ\text{--}45^\circ\text{N}$ ;  $7.5 \text{ m}\cdot\text{s}^{-1}$ ). The direction of the annual mean wind is generally westerly in Mongolia. The magnitude of spatial variability of wind direction in western and northern Mongolia is considerably larger than that in eastern and southern Mongolia. The wind direction is mostly in the range of  $67.5^\circ\text{--}135^\circ$  in eastern and southern Mongolia and  $0^\circ\text{--}180^\circ$  in western and northern Mongolia. The lower wind speed and larger spatial variability of wind direction in western and northern Mongolia are likely to be associated with complex topography in these regions.

As in the annual mean wind speed, the seasonal mean wind speed in eastern and southern Mongolia is higher than that in western and northern Mongolia for all seasons (Figure 4b–e). The direction of the seasonal mean wind in Mongolia is westerly to northwesterly in spring, autumn, and winter. Spring features the highest seasonal mean wind speed ( $5.6 \text{ m}\cdot\text{s}^{-1}$ ) (Figure 4b). Takemi and Seino (2005) suggested that the higher wind speed in spring is caused by a frequent cyclogenesis in spring in Mongolia. Summer is characterized by the lowest seasonal mean wind speed ( $4.5 \text{ m}\cdot\text{s}^{-1}$ ) (Figure 4c). It is interesting to note that the magnitude of the summer mean wind vector is very small despite the considerable summer mean wind speed, especially in eastern and southern Mongolia. This discrepancy will be discussed in detail in section 4.1.2 where the diurnal variation of 100 m wind is described. The seasonal mean wind speed in autumn (Figure 4d) is higher than that in summer but is lower than that in spring. The seasonal mean wind

speed in winter (Figure 4e) is lower than that in autumn in most regions of Mongolia. However, in some regions showing high wind speed (e.g., the two hotspots on the eastern and southern borders), the seasonal mean wind speed in winter is comparable to or even higher than that in spring.

To examine the peak month and amplitude of monthly variation of 100 m wind speed spatially in detail, their spatial distributions are plotted in Figure 5. Here, the coefficient of variation calculated using the 12 monthly mean wind speeds is used to represent the amplitude of monthly variation. In Mongolia, the regions showing an April–May peak are the most common (94%), followed by those showing a November–December peak (6%) (Figure 5a). These regions together cover almost entire Mongolia. The regions showing the November–December peak generally match the regions having particularly high wind speed in winter (Figure 4e). The April–May peak was also reported at 30 m by Elliott et al. (2001) in the regions with lower altitudes in Mongolia. They also reported an October–December peak on ridge crests in western Mongolia, which is different from the result at 100 m in this study. The amplitude of the monthly variation exhibits a considerable difference between the regions in Mongolia (Figure 5b). The amplitude of the monthly variation in eastern and southern Mongolia (0.10) is generally smaller than that in western and northern Mongolia (0.14). In western and northern Mongolia, relatively large amplitudes of the monthly variation appear in the basin between the Altai Mountains and the Khangai Mountains (0.39) and south of the Mongol-Altai Mountains (0.33).

According to the results from Figures 4 and 5b, the wind characteristics in eastern and southern Mongolia are considerably different from those in western and northern Mongolia. Hence, we divide Mongolia into the

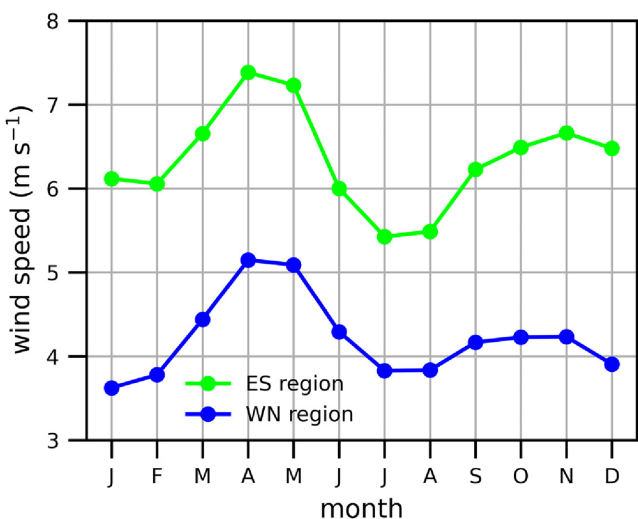


FIGURE 6 Monthly variations of 100 m wind speed averaged over the period 1979–2020 in the ES and WN regions [Colour figure can be viewed at [wileyonlinelibrary.com](http://wileyonlinelibrary.com)]

eastern and southern region (hereafter ES region) and the western and northern region (hereafter WN region) (Figure 1b) and the monthly variation of 100 m wind speed is compared between the two regions in Figure 6. In both the regions, the wind speed exhibits two peaks (April and November) and is highest in April ( $7.4 \text{ m}\cdot\text{s}^{-1}$  for the ES region;  $5.1 \text{ m}\cdot\text{s}^{-1}$  for the WN region). The lowest wind speed is found in July for the ES region ( $5.4 \text{ m}\cdot\text{s}^{-1}$ ) and in January for the WN region ( $3.6 \text{ m}\cdot\text{s}^{-1}$ ). The difference in wind speed between the two regions is largest in December ( $2.6 \text{ m}\cdot\text{s}^{-1}$ ) and is smallest in July ( $1.6 \text{ m}\cdot\text{s}^{-1}$ ), which is consistent with the small difference in wind speed between the two regions in summer (Figure 4c) and the large difference in winter (Figure 4e).

#### 4.1.2 | Diurnal variation

Figure 7 shows the spatial distributions of 100 m wind speed and wind vector averaged over the period 1979–2020 at different times of the day. At all times, the wind speed in eastern and southern Mongolia is higher than that in western and northern Mongolia. The wind direction is generally westerly in Mongolia at all times, showing small diurnal variations in most regions of Mongolia. Large diurnal variations of wind direction are found near the southern border of Mongolia and on southern slopes of mountains such as the Gobi-Altai Mountains and Khangai Mountains. In eastern and southern Mongolia, the wind speed is higher in the night-time (2300–0500 LST) and is lower from the late morning to early afternoon (1100–1400 LST). In western and northern Mongolia, the wind speed is higher in the afternoon

(1400–1700 LST). Previous studies have attributed the night-time enhancement of the mean wind speed above  $\sim 200$  m to the inertial oscillation of ageostrophic wind component and the afternoon enhancement of the mean wind speed below a few tens of meters to the downward momentum transport from upper levels by daytime vertical mixing (e.g., Fajber et al., 2014; Stull, 2011). The phase of diurnal variation of wind speed reverses across a level between them, but the phase-reversal level is different depending on regions (Crawford & Hudson, 1973; Fajber et al., 2014; Mahrt, 1981). The phase of the diurnal variation found in this study suggests that the phase-reversal level in eastern and southern Mongolia is lower than 100 m but that in western and northern Mongolia is higher than 100 m. Further study is needed to find the reason for the difference in the phase-reversal level between the regions in Mongolia.

The peak time and amplitude of diurnal variation of 100 m wind speed are examined spatially in detail in Figure 8. The coefficient of variation calculated using the 24 hourly mean wind speeds is used to represent the amplitude of diurnal variation. For the annual mean diurnal variation of wind speed (Figure 8a), the majority of regions in eastern and southern Mongolia show an evening-to-night peak (1900–0300 LST) and that in western and northern Mongolia show an afternoon peak (1400–1800 LST). Some regions in eastern Mongolia exhibit a dawn-to-morning peak (0600–0800 LST), and some other regions with lower altitudes in western and northern Mongolia exhibit an evening peak (1900–2300 LST). The amplitude of the annual mean diurnal variation of wind speed is generally smaller in eastern and southern Mongolia (0.06) than in western and northern Mongolia (0.10) (Figure 8b), as in that of the monthly variation (Figure 5b). However, the location showing a large amplitude of the diurnal variation is different from that of the monthly variation: the western and southern slopes of mountains such as the Mongol-Altai Mountains, Gobi-Altai Mountains and Khangai Mountains. The spatial pattern of the peak time considerably varies with the season (Figure 8c–f). In spring (Figure 8c), the afternoon peak prevails across Mongolia, accounting for 74% of Mongolia. In summer (Figure 8d), in contrast with spring, the regions showing the evening-to-night peak account for the majority of Mongolia (55%). The afternoon peak appears mostly in the mountainous regions such as the Mongol-Altai Mountains, Khangai Mountains, Khentii Mountains and eastern Sayan Mountains. The dawn-to-morning peak in the eastern region almost disappears in summer. The spatial pattern of the peak time in autumn is similar to that in summer, except the reoccurrence of the dawn-to-morning peak in the eastern regions and a slight decrease in area of the

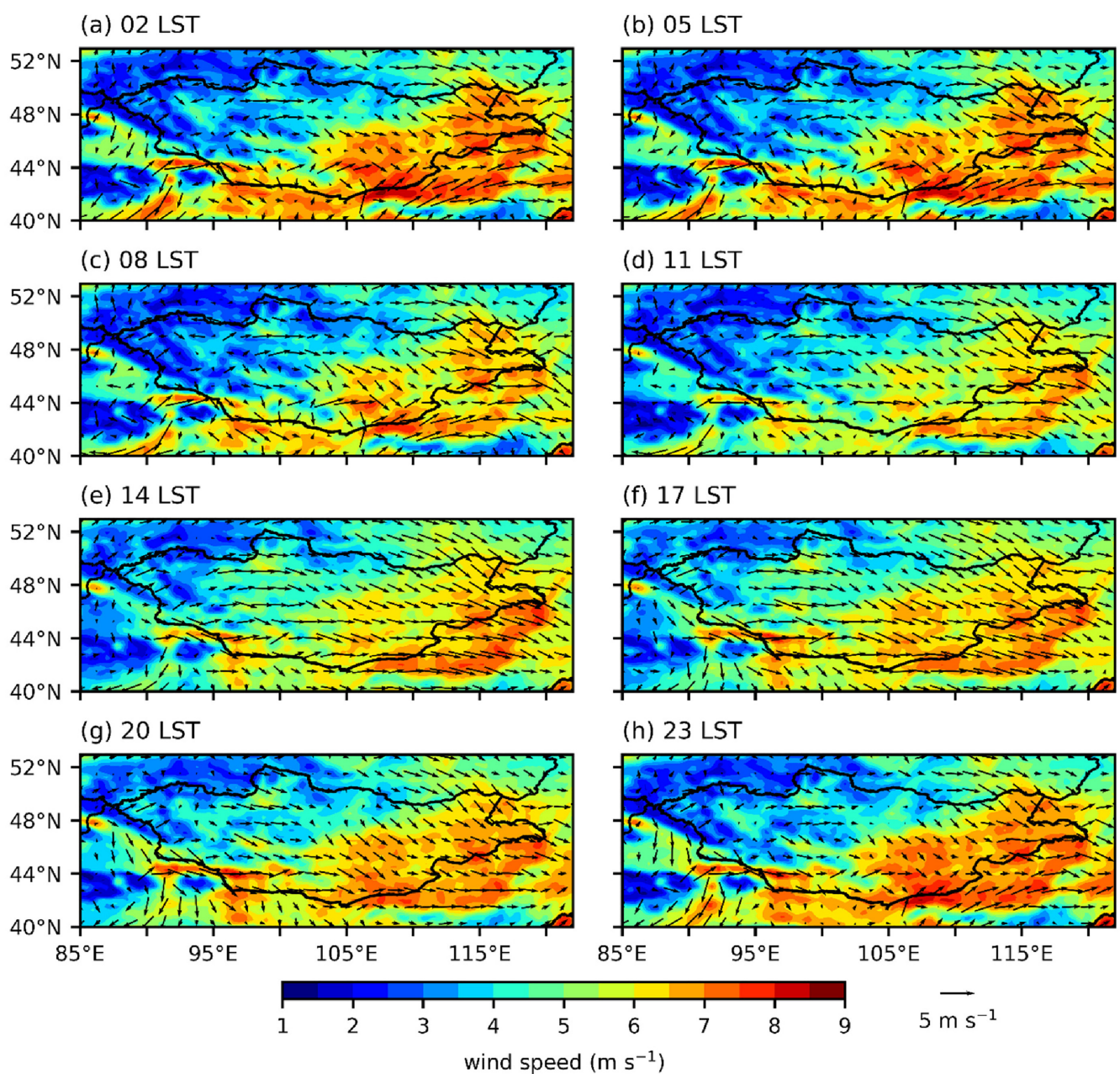


**FIGURE 7** Spatial distributions of 100 m wind speed (shades) and wind vector (arrows) averaged over the period 1979–2020 at different times of the day [Colour figure can be viewed at [wileyonlinelibrary.com](http://wileyonlinelibrary.com)]

regions showing the evening-to-night peak (Figure 8e). In winter (Figure 8f), patchy regions showing dawn-to-morning peaks suddenly appear mainly in western and northern Mongolia, which increases the spatial heterogeneity of peak time in winter.

Considering the difference in the peak time between eastern and southern Mongolia and western and northern Mongolia (Figure 8a), the diurnal variation of 100 m wind speed is compared between the ES and WN regions for each season in Figure 9a–d. Note that there are some eastern regions where the dawn-to-morning peak appears unlike the rest part of the ES region where the evening-

to-night peak appears, but these regions have the diurnal variation of wind speed that is similar to that in the ES region (not shown). The ES region features high nighttime wind speed that continues for a long time in all seasons, while the WN region is characterized by an afternoon peak after which the wind speed rapidly decreases in all seasons except summer. In spring (Figure 9a), the ES region shows an afternoon peak of wind speed (1600 LST) as well as its characteristic high wind speed at night. This afternoon peak in the ES region is found only in spring. Similarly, the wind speed in the WN region shows the most pronounced afternoon peak

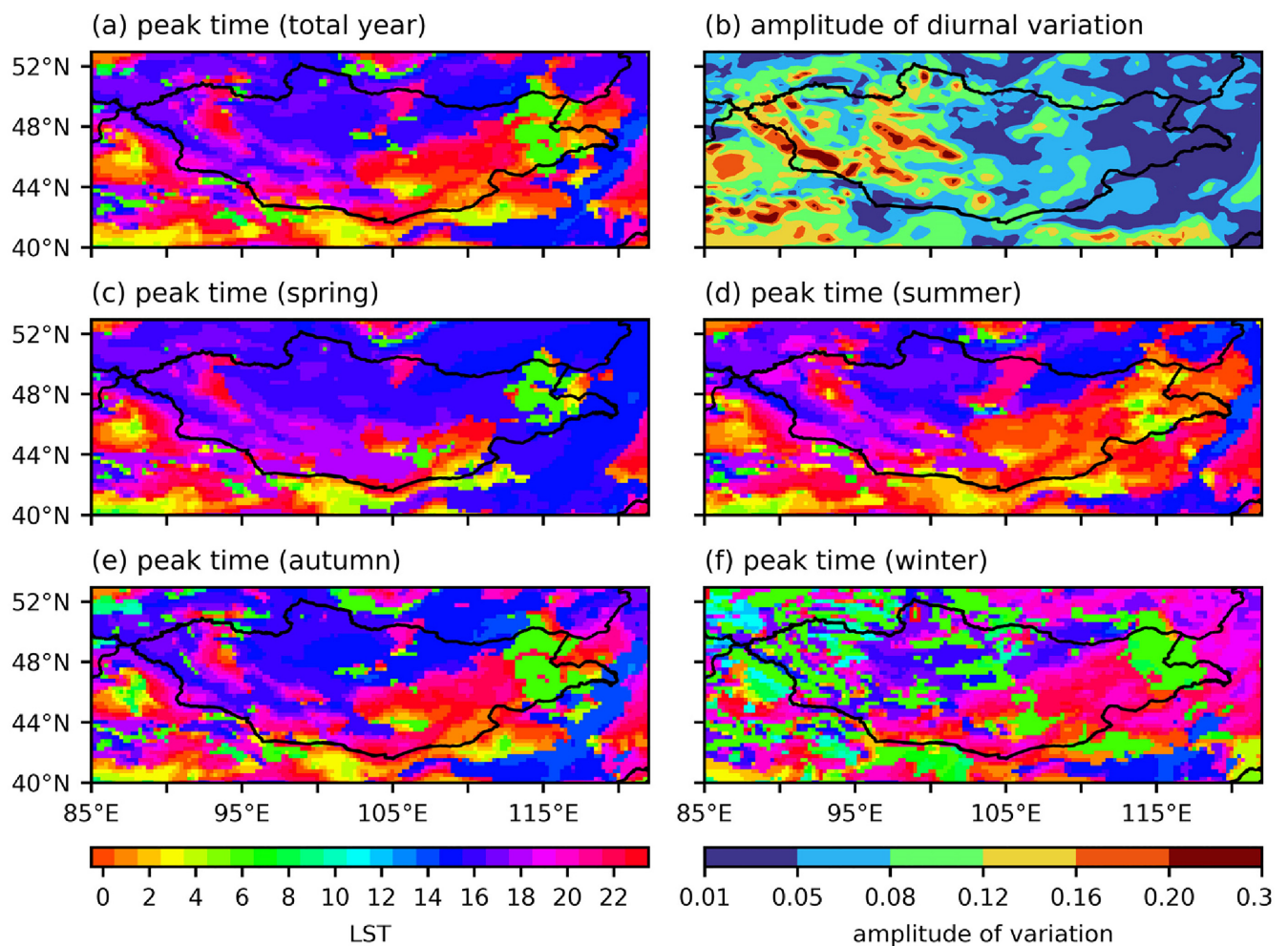


**FIGURE 8** Spatial distributions of peak time of diurnal variation for 100 m wind speed averaged over (a) the whole year, (c) spring, (d) summer, (e) autumn and (f) winter during the period 1979–2020. (b) Spatial distribution of amplitude of diurnal variation for 100 m wind speed averaged over the period 1979–2020 [Colour figure can be viewed at [wileyonlinelibrary.com](http://wileyonlinelibrary.com)]

(1700 LST) in spring among all seasons. The minimum wind speed appears in the morning (0900 LST) in both the regions. In summer (Figure 9b), the wind speed in the ES region shows maximum at midnight (2400 LST) and that in the WN region shows a late-afternoon peak (1800 LST). The amplitude of the diurnal variation in the WN region in summer is second largest among those in all seasons. The minimum wind speed in summer appears in the morning (0900 LST) in both the regions, as in spring (Figure 9a). The diurnal variation of wind speed in autumn is qualitatively similar to that in summer (Figure 9c). The maximum wind speed occurs around midnight (2300 LST) and in the afternoon (1600 LST) in the ES and WN regions, respectively, and the minimum wind speed appears in the morning (1000 LST) in both the regions. The diurnal variation of wind speed in winter is similar to that in summer and autumn for the ES region (Figure 9d). However, for the WN region, the diurnal variation in winter is

considerably different from those in other seasons, showing almost constant wind speed during 1500–0900 LST. This constant wind speed is represented as the large heterogeneity of peak time in western and northern Mongolia in winter (Figure 8f). In both the regions, the minimum wind speed in winter appears at noon, which is 3 (2) hours later than the time of the minimum wind speed in spring and summer (autumn).

For the wind direction, both the regions show westerly in all seasons except summer, and the diurnal variations of wind direction in these seasons are small ( $<25^\circ$ ) (not shown). However, in summer, the wind direction varies considerably with time in both the regions (Figure 9e). The wind direction in the ES region rotates clockwise once a day, being easterly at 0000 LST, southerly at 0300 LST, westerly at 0500 LST and northerly at 2000 LST. The wind direction in the WN region also shows a significant amplitude of diurnal variation ( $66^\circ$ ), being almost northerly at 0000 LST and westerly at

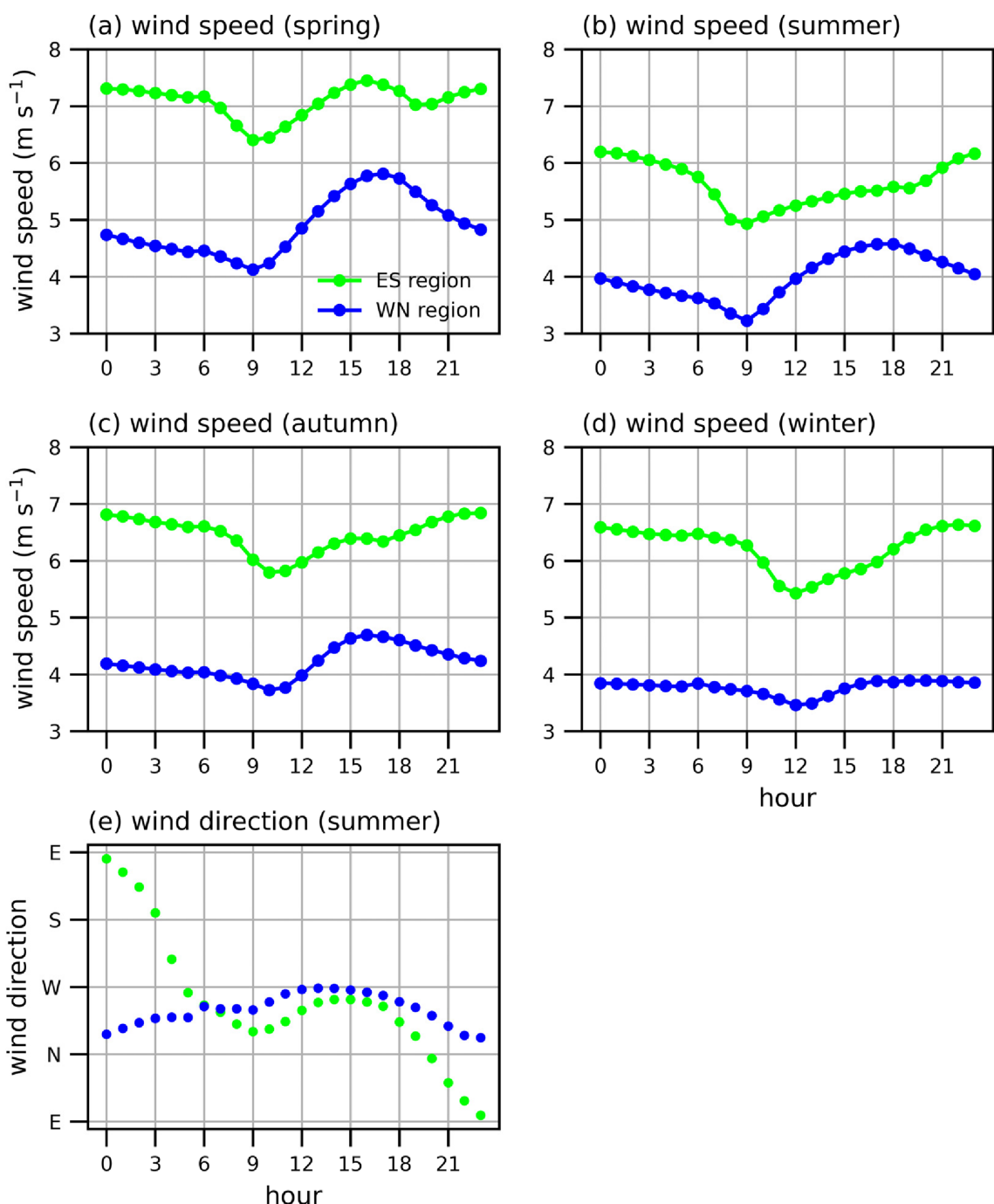


**FIGURE 9** Diurnal variations of 100 m wind speed averaged over the period 1979–2020 in the ES and WN regions for (a) spring, (b) summer, (c) autumn and (d) winter. (e) Diurnal variations of direction of 100 m wind averaged over the period 1979–2020 in the ES and WN regions for summer [Colour figure can be viewed at [wileyonlinelibrary.com](http://wileyonlinelibrary.com)]

1200 LST. These large diurnal variations of wind direction in summer are responsible for the large discrepancy between the summer mean wind speed and the magnitude of summer mean wind vector (Figure 4c).

During past decades, climate change has been significantly modifying regional climates. Because Mongolia is known as one of the countries that experience the most severe global warming (IPCC, 2018), the long-term changes in meteorological variables including the near-surface wind speed and their associations with climate

change deserve future investigation using a variety of observation and reanalysis datasets.

#### 4.2 | Assessment of wind energy potential

In this subsection, the wind energy potential at 100 m in Mongolia is assessed based on the wind class and wind energy metrics. Figure 10a shows the map of wind class

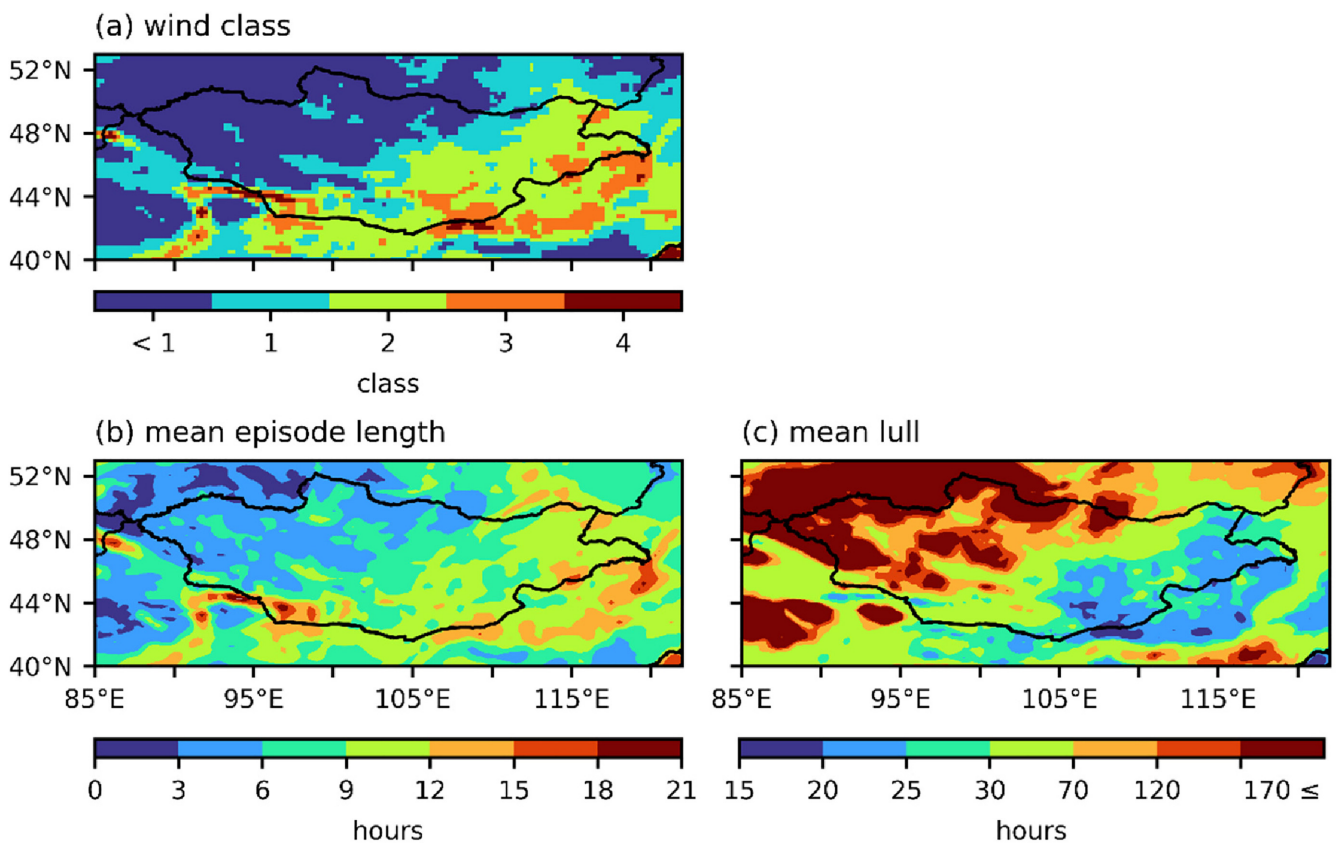


**FIGURE 10** Spatial distributions of (a) wind class, (b) mean episode length and (c) mean lull for 100 m wind power density during the period 1979–2020. The wind classes are assigned based on the annual mean wind power density. In the colour bar in (a), ‘<1’ indicates the wind power density lower than the lower boundary of Class 1 [Colour figure can be viewed at [wileyonlinelibrary.com](http://wileyonlinelibrary.com)]

determined by the annual mean wind power density. The wind energy resources at the four hotspots (Figure 4a) belong to Class 3 or above, which are good for utility application and excellent for rural application (Table 1). The wind energy resources in most regions of eastern and southern Mongolia are, at least, good for rural application (i.e., Class 2 or above). Figure 11 shows the monthly and diurnal variations of 100 m wind power density in the ES and WN regions. The wind energy resources in the ES region correspond to Class 2, but they rise up to Class 3 in April and May and fall to Class 1 in July and August. In terms of diurnal variation, the wind energy resources in the ES region is about a half class higher in the night-time than in the daytime, except in spring when the diurnal maximum of wind speed appears in the afternoon (Figure 9a). Unlike the wind energy resources in the ES region, those in the WN region are moderately applicable at best in March–May and November, even for rural application. Note that in the ES region, summer is the least favourable season for 100 m wind power generation due to the insufficient wind energy resources (Figure 11) and largest diurnal variability of wind direction in this season (Figure 9e).

In addition to the abundance (i.e., wind class), the variability and intermittency of wind energy resources are also examined due to the importance of stability of wind power generation. The small amplitudes of monthly and diurnal variations of wind speed in eastern and southern Mongolia (Figures 5b and 8b) indicate that the wind energy resources in eastern and southern Mongolia are more stable than those in western and northern Mongolia. Comparing eastern and southern Mongolia, the amplitude of the monthly variation is smaller in southern Mongolia and that of the diurnal variation is smaller in eastern Mongolia. The mean episode length is longer in eastern and southern Mongolia (about 10 h) than in western and northern Mongolia (about 7 h) (Figure 10b). Comparing eastern and southern Mongolia, the mean episode length in eastern Mongolia is slightly longer than that in southern Mongolia. As expected, the four hotspots of wind speed (Figure 4a) exhibit long mean episode lengths (>12 h). Among the four hotspots, the one located south of the Gobi-Altai Mountains has the longest mean episode length (21 h). The mean lull is shorter in eastern and southern Mongolia (about 28 h) than in western and northern Mongolia (about 203 h) (Figure 10c).

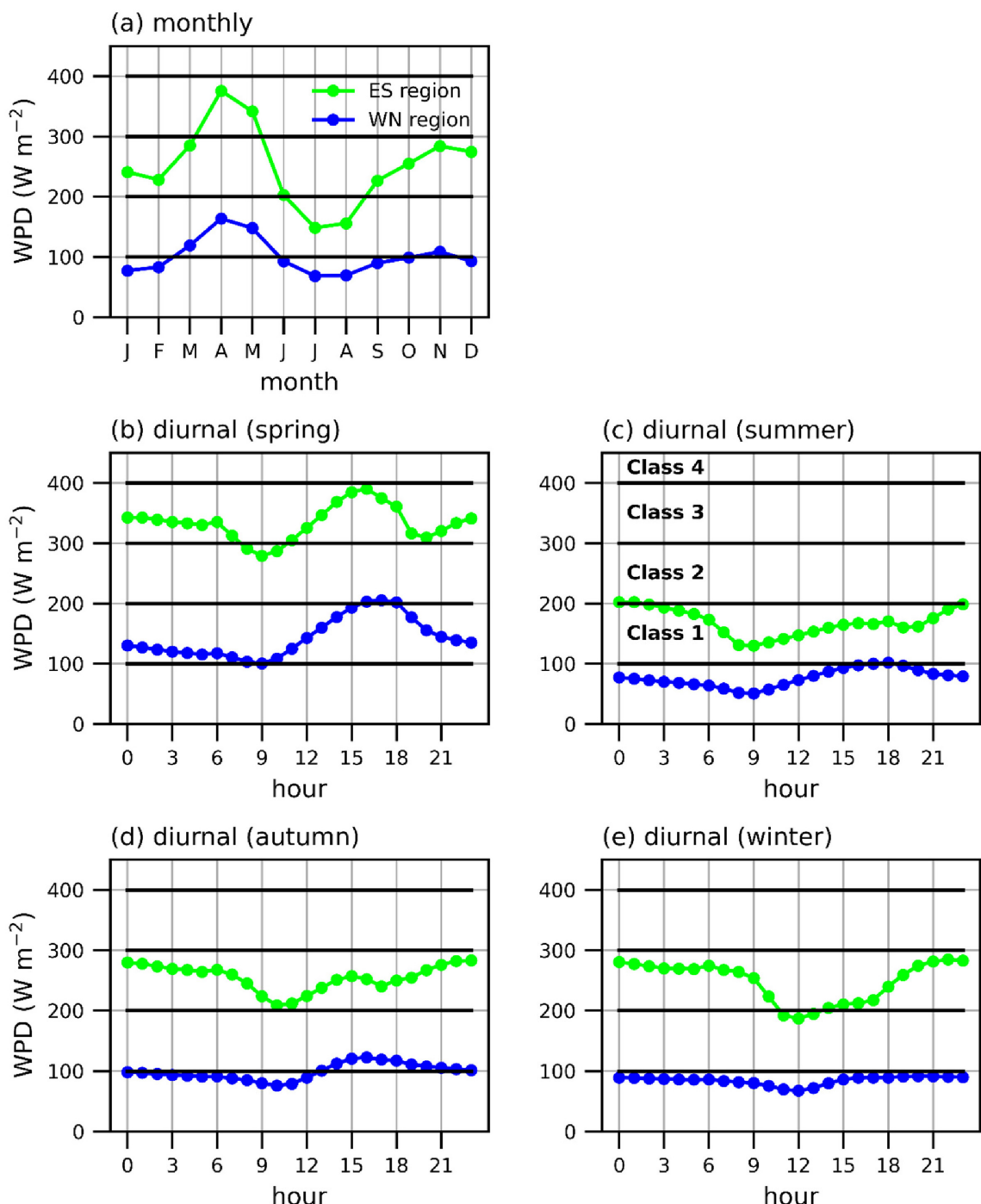


**FIGURE 11** (a) Monthly variations of 100 m wind power density averaged over the period 1979–2020 in the ES and WN regions. Diurnal variations of 100 m wind power density averaged over the period 1979–2020 in the ES and WN regions for (b) spring, (c) summer, (d) autumn and (e) winter [Colour figure can be viewed at [wileyonlinelibrary.com](http://wileyonlinelibrary.com)]

The above analyses that the amount of wind energy resources is generally larger in eastern and southern Mongolia than in western and northern Mongolia are consistent with the results of Elliott et al. (2001). However, the existence of high wind speeds on some mountain tops or ridges reported by Elliott et al. (2001) is not found in this study. The

absence of high wind speeds on mountain tops or ridges in this study may be related to the spatial resolution of the ERA5 data which is not fine enough to fully represent the local flows over complex terrains (Dörenkämper et al., 2020; Gualtieri, 2022). To estimate wind energy resources on the mountain tops or ridges in detail, high-resolution numerical simulations

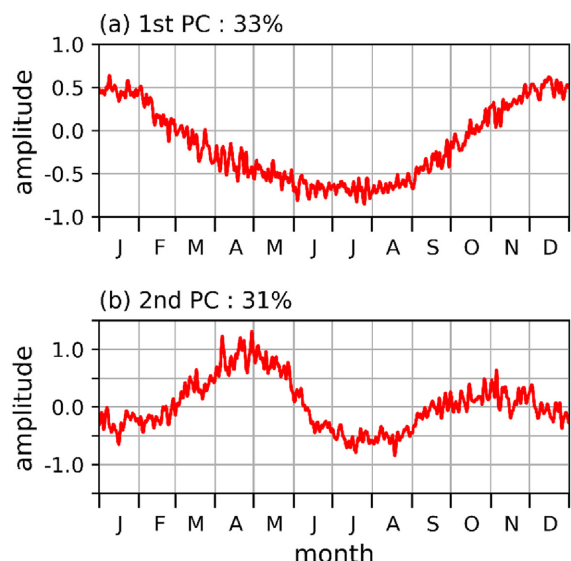


**FIGURE 12** PC time series for the (a) first and (b) second CSEOF modes of 100 m wind speed anomaly [Colour figure can be viewed at [wileyonlinelibrary.com](http://wileyonlinelibrary.com)]

for a long-term period or a dense observation network is needed.

### 4.3 | Possible mechanisms for 100 m wind variation

Using the CSEOF analysis method, the variation of 100 m wind speed anomaly in Mongolia is decomposed into multiple modes. Among them, two principal modes explain a large portion of the total variation. The PC time series of the two CSEOF modes are shown in Figure 12. Each mode shows a distinct seasonal variation of the PC time series. The first mode, which contributes 33% to the total variance, is amplified with positive values in the PC time series in winter and is amplified with negative values in summer. The second mode, which contributes 31% to the total variance, has the PC time series that shows two peaks in spring and autumn, which resembles the seasonal variation of 100 m wind speed itself (Figure 6).

The CSLV for each mode is the decomposed diurnally varying spatial pattern of 100 m wind speed anomaly. Figure 13 shows the CSLV for the first mode. It is characterized by positive wind speed anomalies in eastern Mongolia maximized at 0800 LST and negative wind speed anomalies in western Mongolia that are prominent in the daytime and minimized at 1700 LST. The regressed CSLV of wind vector anomaly shows that the positive wind speed anomalies in eastern Mongolia correspond to the northwesterlies and westerlies during the night-time, which turn clockwise outside the southeast boundary of Mongolia. Given that this mode is amplified in winter

with positive values in the PC time series (Figure 12a), this mode is strongly associated with the wintertime northwesterlies and westerlies in eastern Mongolia (Figure 4e). Considering that the PC time series of this mode changes its sign and is amplified with negative values in summer, the negative wind speed anomalies in western Mongolia seen in the CSLV indicate a positive contribution to the 100 m wind speed there in summer by the northwesterlies, which suggests that this mode is also associated with the summertime northwesterlies along the southwest boundary of Mongolia (Figure 4c).

The first CSEOF mode is deeply associated with the seasonal reversal of the East Asian monsoon. Figure 14 shows the regressed CSLV of geopotential height anomaly and wind vector anomaly at 700 hPa. At all times, the western part of Mongolia shows a relatively high geopotential height anomaly and strong clockwise winds surround the anomaly, blowing southeastward to eastern China, Korea and Japan. In winter, this geopotential height anomaly indicates the Siberian High and the wind anomaly pattern corresponds to the East Asian winter monsoon. The annual mean 700 hPa wind is northwestly in Mongolia, and eastern Mongolia experiences strong northwesterlies at 700 hPa in this season. The strong monsoonal northwesterlies are responsible for the spatial maximum of 100 m wind speed in southeastern Mongolia in winter. In summer, the wind anomaly pattern is reversed, showing southeasterly anomalies toward eastern Mongolia, as a part of the East Asian summer monsoon. The southeasterly anomalies in summer against the annual mean northwesterlies indicate relatively low mean wind speed at 700 hPa in this season.

The second CSLV of 100 m wind speed anomaly is presented in Figure 15. In this mode, strong wind speed anomalies appear in the mountainous regions such as the Khangai Mountains, Khentii Mountains and Greater Khingan Mountains in the afternoon. In the night-time, the basin between the Khentii Mountains and Greater Khingan Mountains and the basin between the Altai Mountains and Khangai Mountains show relatively strong wind speed anomalies compared to the surrounding regions, although they are not strong as those in the mountainous regions in the afternoon. These relationships between the wind speed anomaly and topography imply that this mode is associated with the mountain-plains solenoid (MPS) circulations (e.g., Bao & Zhang, 2013; Wolyn & McKee, 1994) and the resultant vertical mixing of momentum. In the afternoon, the differential heating between the mountains and plains generates winds that converge to the mountains and thus convection over the mountains. The vertical mixing in this region induces the downward momentum transport from the relatively strong winds at the upper levels,

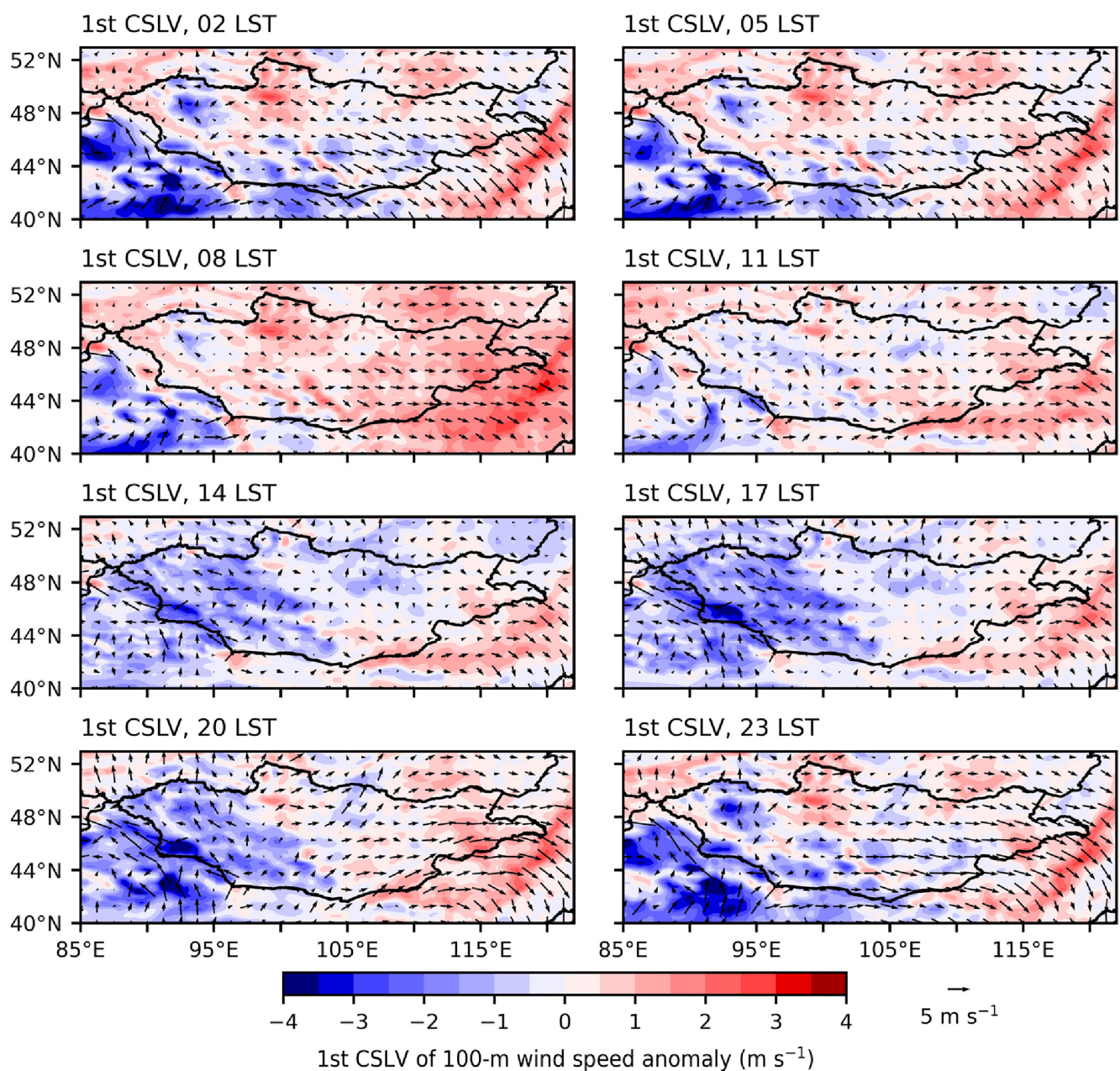


**FIGURE 13** CSLV for the first CSEOF mode of 100 m wind speed anomaly (shades) and regressed CSLV of 100 m wind vector anomaly [Colour figure can be viewed at [wileyonlinelibrary.com](http://wileyonlinelibrary.com)]

enhancing the surface wind speed (Miyazaki et al., 1999). This explains the strong wind speed anomalies in the mountainous regions that appear in the afternoon. In the night-time, downslope winds induced by the differential cooling between the mountains and basins cause low-level convergence over the basins between the mountains, generating convection there. This explains the strong wind speed anomalies in the basins. This mode is almost deactivated in winter (Figure 12b) because the lower atmosphere is too stable due to the cold surface and strong Siberian High, and it is activated in spring when the strong stability of the lower atmosphere is

reduced. This mode is deactivated again in summer despite the reduced stability, possibly because of the relatively low mean wind speed aloft in this season (Figure 14), which results in decreases in the downward momentum transport from the upper levels.

In spring and autumn when the second CSEOF mode is amplified, there are frequent passages of extratropical cyclones over Mongolia (Lee et al., 2020). The extratropical cyclones may have some effects on near-surface wind in Mongolia and its spatiotemporal variation, but the effects are not clearly captured in the CSEOF analysis in this study. With regard to this, further investigation that

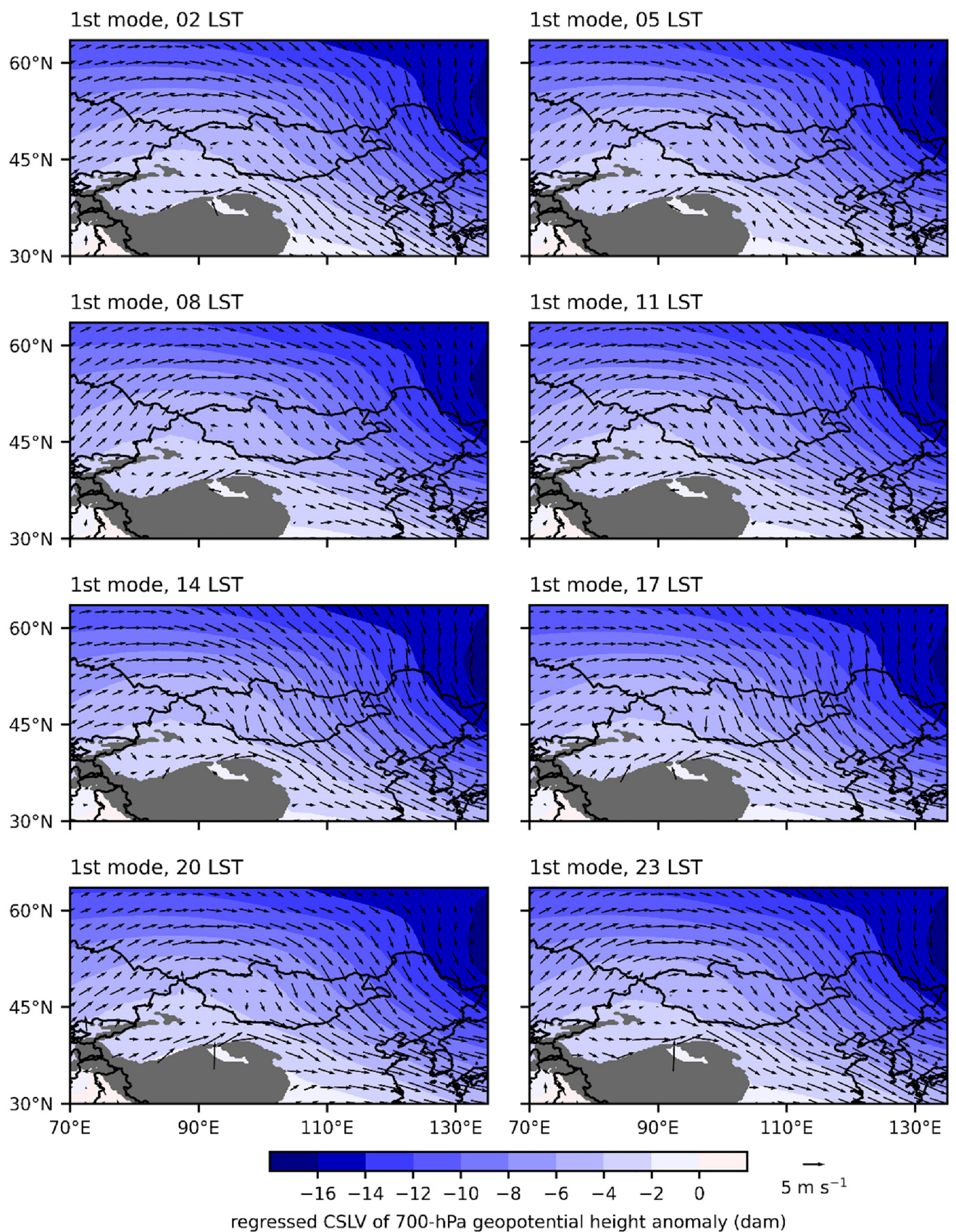


**FIGURE 14** Regressed CSLV of 700 hPa geopotential height and wind vector anomaly associated with the first CSEOF mode of 100 m wind speed anomaly. The area where the surface pressure is lower than 700 hPa at any time in the 1-year-length mean data is masked in grey [Colour figure can be viewed at [wileyonlinelibrary.com](http://wileyonlinelibrary.com)]

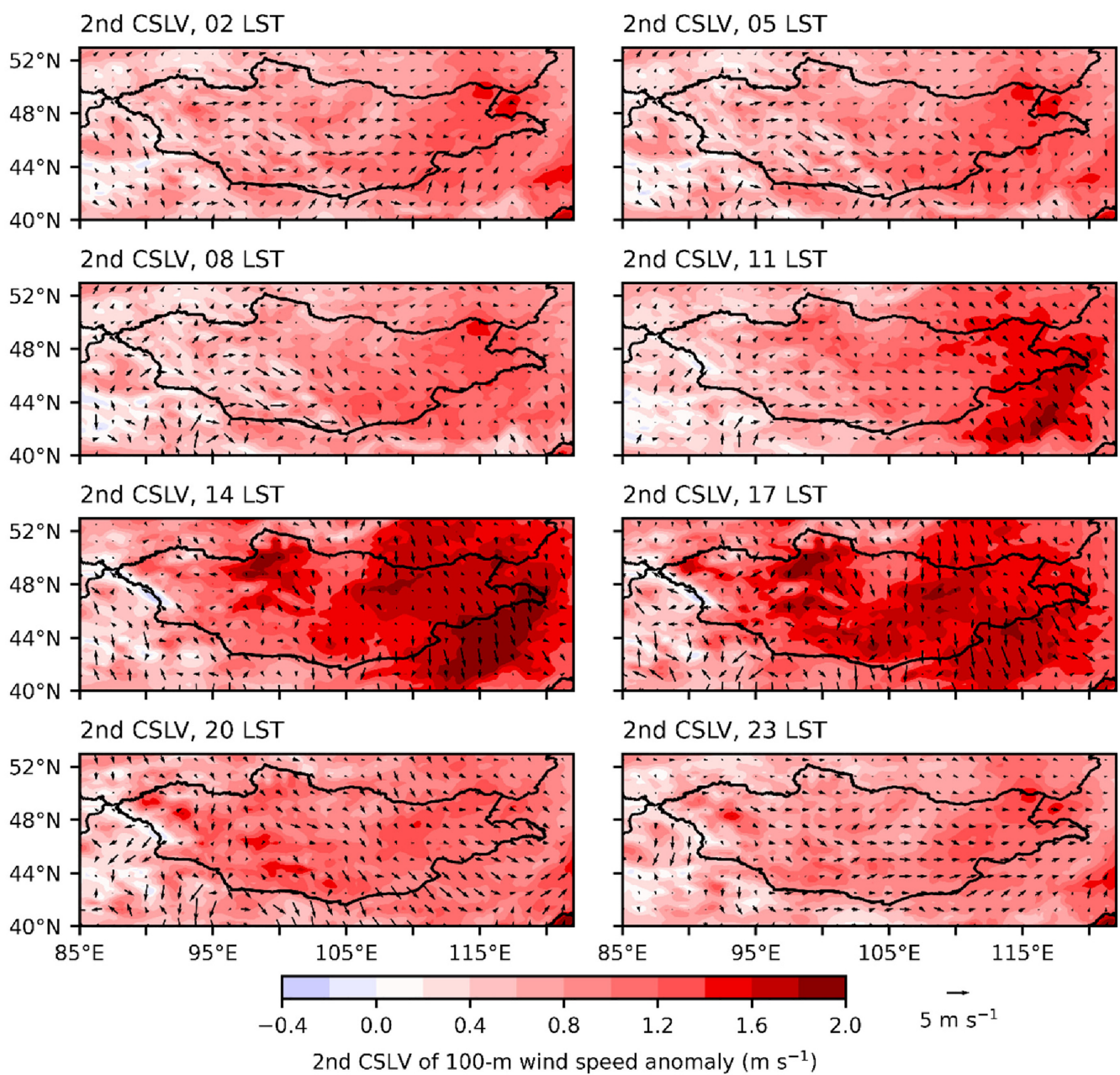


**FIGURE 15** As in Figure 13, but for the second CSEOF mode of 100 m wind speed anomaly [Colour figure can be viewed at [wileyonlinelibrary.com](http://wileyonlinelibrary.com)]

looks into the effect of individual extratropical cyclone on near-surface wind in Mongolia may be needed.

## 5 | SUMMARY AND CONCLUSIONS

The spatiotemporal variations of 100 m wind in Mongolia are investigated with attention to wind energy resources. For this, the ERA5 data during 1979–2020 are used. The monthly variation of 100 m wind in Mongolia has two peaks in April and November, where the April peak is

higher. The eastern and southern (ES) region and the western and northern (WN) region of the country exhibit different 100 m wind characteristics. In the ES region, the wind speed is relatively high and maximizes in the nighttime and its monthly and diurnal variations have relatively small amplitudes. This region is classified to have good potential for wind energy development with a long mean episode length. In the WN region, the wind speed is relatively low and maximizes in the afternoon and its monthly and diurnal variations have relatively large amplitudes. This region is classified to have less wind energy potential. We found four spots of the greatest wind energy

potential, which are near the eastern border of Mongolia, south of the Gobi-Altai Mountains, near the southern border of Mongolia and in the southern region. The spatiotemporal variations of 100 m wind speed are decomposed into multiple modes using the CSEOF analysis method, and the two principal modes are analysed. The first CSEOF mode shows a seasonally reversing time series and an east–west contrast, which is associated with the seasonal change of the East Asian monsoon. The second mode shows two peaks in spring and autumn and exhibits mountain–basin contrasts that are reversed diurnally, which may be associated with the mountain–plains solenoid circulations and resultant vertical mixing of momentum.

This study suggests possible contributors to the spatiotemporal variations of 100 m wind speed in Mongolia such as the East Asian monsoon and local circulation, but does not examine the specific dynamics and physics through which each of the contributors affects near-surface wind, which requires further investigation. For example, numerical simulations of the diurnal evolution of 100 m wind speed when the East Asian winter monsoon is predominant over Mongolia can be conducted to better understand the mechanisms for spatiotemporal variations of 100 m wind speed in winter.

## AUTHOR CONTRIBUTIONS

**Seong-Ho Hong:** Formal analysis; investigation; visualization; writing – original draft. **Jambajamts Lkhamjav:** Formal analysis; investigation; visualization; writing – original draft. **Han-Gyul Jin:** Formal analysis; writing – original draft; writing – review and editing. **Jong-Jin Baik:** Conceptualization; formal analysis; project administration; supervision; writing – review and editing.

## ACKNOWLEDGEMENTS

The authors thank the National Agency Meteorology and the Environmental Monitoring of Mongolia for providing the surface wind data. The authors also thank the two anonymous reviewers who provided valuable comments on this work. Jambajamts Lkhamjav is supported by the Chey Institute for Advanced Studies' International Scholar Exchange Fellowship for the academic year of 2021–2022 and by the National University of Mongolia under grant NUM-P20193744.

## CONFLICT OF INTEREST STATEMENT

The authors declare no conflicts of interest.

## ORCID

Jong-Jin Baik  <https://orcid.org/0000-0003-3709-0532>

## REFERENCES

- Abdou, K., Parker, D.J., Brooks, B., Kalthoff, N. & Lebel, T. (2010) The diurnal cycle of lower boundary-layer wind in the West African monsoon. *Quarterly Journal of the Royal Meteorological Society*, 136, 66–76. Available from: <https://doi.org/10.1002/qj.536>
- Bao, X. & Zhang, F. (2013) Impacts of the mountain–plains solenoid and cold pool dynamics on the diurnal variation of warm-season precipitation over northern China. *Atmospheric Chemistry and Physics*, 13, 6965–6982. Available from: <https://doi.org/10.5194/acp-13-6965-2013>
- Boudia, S.M. & Santos, J.A. (2019) Assessment of large-scale wind resource features in Algeria. *Energy*, 189, 116299. Available from: <https://doi.org/10.1016/j.energy.2019.116299>
- Chen, Y., Göntü, G. & Tumenjargal, M. (2016) *Renewables readiness assessment: Mongolia*. Abu Dhabi: International Renewable Energy Agency. Available from: <https://www.irena.org/publications/2016/Mar/Renewables-Readiness-Assessment-Mongolia>
- Crawford, K.C. & Hudson, H.R. (1973) The diurnal wind variation in the lowest 1500 ft in Central Oklahoma: June 1966–May 1967. *Journal of Applied Meteorology and Climatology*, 12, 127–132. Available from: [https://doi.org/10.1175/1520-0450\(1973\)012<0127:TDWVIT>2.0.CO;2](https://doi.org/10.1175/1520-0450(1973)012<0127:TDWVIT>2.0.CO;2)
- Dörenkämper, M., Olsen, B.T., Witha, B., Hahmann, A.N., Davis, N.N., Barcons, J. et al. (2020) The making of the new European wind atlas—part 2: production and evaluation. *Geoscientific Model Development*, 13, 5079–5102. Available from: <https://doi.org/10.5194/gmd-13-5079-2020>
- ECMWF. (2021) *IFS Documentation Cy47r3—part IV: physical processes*. Reading: ECMWF. Available from: <https://doi.org/10.21957/eyrpir4v4>
- Elliott, D., Schwartz, M., Scott, G., Haymes, S., Heimiller, D. & George, R. (2001) *Wind energy resource atlas of Mongolia*. Golden, CO: National Renewable Energy Laboratory. Available from: <https://www.nrel.gov/docs/fy0losti/28972.pdf>
- Fajber, R., Monahan, A.D. & Merryfield, W.J. (2014) At what time of day do daily extreme near-surface wind speeds occur? *Journal of Climate*, 27, 4226–4244. Available from: <https://doi.org/10.1175/JCLI-D-13-00286.1>
- Gualtieri, G. (2022) Analysing the uncertainties of reanalysis data used for wind resource assessment: a critical review. *Renewable and Sustainable Energy Reviews*, 167, 112741. Available from: <https://doi.org/10.1016/j.rser.2022.112741>
- Gubbala, C.S., Dodla, V.B.R. & Desamsetti, S. (2021) Assessment of wind energy potential over India using high-resolution global reanalysis data. *Journal of Earth System Science*, 130, 64. Available from: <https://doi.org/10.1007/s12040-021-01557-7>
- Hersbach, H., Bell, B., Berrisford, P., Hirahara, S., Horányi, A., Muñoz-Sabater, J. et al. (2020) The ERA5 global reanalysis. *Quarterly Journal of the Royal Meteorological Society*, 146, 1999–2049. Available from: <https://doi.org/10.1002/qj.3803>
- IPCC. (2018) *Climate change 2013: the physical science basis*. Cambridge: Cambridge University Press. Available from: <https://www.ipcc.ch/report/ar5/wg1/>
- Kalnay, E., Kanamitsu, M., Kistler, R., Collins, W., Deaven, D., Gandin, L. et al. (1996) The NCEP/NCAR 40-year reanalysis project. *Bulletin of the American Meteorological Society*, 77, 437–

472. Available from: [https://doi.org/10.1175/1520-0477\(1996\)077<0437:TNYRP>2.0.CO;2](https://doi.org/10.1175/1520-0477(1996)077<0437:TNYRP>2.0.CO;2)
- Kim, K.-Y. (2017) *Cyclostationary EOF analysis: theory and applications*. Seoul: Seoul National University Press.
- Kim, K.-Y. & North, G.R. (1997) EOFs of harmonizable cyclostationary processes. *Journal of the Atmospheric Sciences*, 54, 2416–2427. Available from: [https://doi.org/10.1175/1520-0469\(1997\)054<2416:EOHCP>2.0.CO;2](https://doi.org/10.1175/1520-0469(1997)054<2416:EOHCP>2.0.CO;2)
- Lantz, E., Roberts, O., Nunemaker, J., DeMeo, E., Dykes, K. & Scott, G. (2019) *Increasing wind turbine tower heights: opportunities and challenges*. Golden, CO: National Renewable Energy Laboratory. Available from: <https://www.energy.gov/eere/wind/downloads/increasing-wind-turbine-tower-heights-opportunities-and-challenges>
- Lee, J., Son, S.-W., Cho, H.-O., Kim, J., Cha, D.-H., Gyakum, J.R. et al. (2020) Extratropical cyclones over East Asia: climatology, seasonal cycle, and long-term trend. *Climate Dynamics*, 54, 1131–1144. Available from: <https://doi.org/10.1007/s00382-019-05048-w>
- Mahrt, L. (1981) The early evening boundary layer transition. *Quarterly Journal of the Royal Meteorological Society*, 107, 329–343. Available from: <https://doi.org/10.1002/qj.49710745205>
- Miyazaki, S., Yasunari, T. & Adyasuren, T. (1999) Abrupt seasonal changes of surface climate observed in Northern Mongolia by an automatic weather station. *Journal of the Meteorological Society of Japan*, 77, 583–593. Available from: [https://doi.org/10.2151/jmsj1965.77.2\\_583](https://doi.org/10.2151/jmsj1965.77.2_583)
- Mulder, F.M. (2014) Implication of diurnal and seasonal variations in renewable energy generation for large scale energy storage. *Journal of Renewable and Sustainable Energy*, 6, 033105. Available from: <https://doi.org/10.1063/1.4874845>
- Natsagdorj, L., Jugder, D. & Chung, Y.S. (2003) Analysis of dust storms observed in Mongolia during 1937–1999. *Atmospheric Environment*, 37, 1401–1411. Available from: [https://doi.org/10.1016/S1352-2310\(02\)01023-3](https://doi.org/10.1016/S1352-2310(02)01023-3)
- Nezhad, M.M., Neshat, M., Groppi, D., Marzialetti, P., Heydari, A., Sylaios, G. et al. (2021) A primary offshore wind farm site assessment using reanalysis data: a case study for Samothraki Island. *Renewable Energy*, 172, 667–679. Available from: <https://doi.org/10.1016/j.renene.2021.03.045>
- Olauson, J. (2018) ERA5: the new champion of wind power modelling? *Renewable Energy*, 126, 322–331. Available from: <https://doi.org/10.1016/j.renene.2018.03.056>
- Pryor, S.C. & Barthelmie, R.J. (2021) A global assessment of extreme wind speeds for wind energy applications. *Nature Energy*, 6, 268–276. Available from: <https://doi.org/10.1038/s41560-020-00773-7>
- Ramon, J., Lledó, L., Torralba, V., Soret, A. & Doblas-Reyes, F.J. (2019) What global reanalysis best represents near-surface winds? *Quarterly Journal of the Royal Meteorological Society*, 145, 3236–3251. Available from: <https://doi.org/10.1002/qj.3616>
- Ren, G., Wan, J., Liu, J. & Yu, D. (2019) Characterization of wind energy resource in China from a new perspective. *Energy*, 167, 994–1010. Available from: <https://doi.org/10.1016/j.energy.2018.11.032>
- Saha, S., Moorthi, S., Pan, H.-L., Wu, X., Wang, J., Nadiga, S. et al. (2010) The NCEP climate forecast system reanalysis. *Bulletin of the American Meteorological Society*, 91, 1015–1058. Available from: <https://doi.org/10.1175/2010BAMS3001.1>
- Shu, Z.R., Li, Q.S., Chan, P.W. & He, Y.C. (2020) Seasonal and diurnal variation of marine wind characteristics based on lidar measurements. *Meteorological Applications*, 27, e1918. Available from: <https://doi.org/10.1002/met.1918>
- Stull, R. (2011) *Meteorology for scientists and engineers*. Vancouver, BC: The University of British Columbia.
- Takemi, T. & Seino, N. (2005) Dust storms and cyclone tracks over the arid regions in East Asia in spring. *Journal of Geophysical Research*, 110, D18S11. Available from: <https://doi.org/10.1029/2004JD004698>
- Wolyn, P.G. & McKee, T.B. (1994) The mountain–plains circulation east of a 2-km-high north–south barrier. *Monthly Weather Review*, 122, 1490–1508. Available from: [https://doi.org/10.1175/1520-0493\(1994\)122<1490:TMPCCEO>2.0.CO;2](https://doi.org/10.1175/1520-0493(1994)122<1490:TMPCCEO>2.0.CO;2)
- Yembuu, B. (2020) *The physical geography of Mongolia*. Cham: Springer.
- Yu, L., Zhong, S., Bian, X. & Heilman, W.E. (2016) Climatology and trend of wind power resources in China and its surrounding regions: a revisit using climate forecast system reanalysis data. *International Journal of Climatology*, 36, 2173–2188. Available from: <https://doi.org/10.1002/joc.4485>
- Yu, R., Li, J. & Chen, H. (2009) Diurnal variation of surface wind over central eastern China. *Climate Dynamics*, 33, 1089–1097. Available from: <https://doi.org/10.1007/s00382-008-0478-3>
- Zhang, Y., Ding, Y. & Li, Q. (2012) A climatology of extratropical cyclones over East Asia during 1958–2001. *Acta Meteorologica Sinica*, 26, 261–277. Available from: <https://doi.org/10.1007/s13351-012-0301-2>

**How to cite this article:** Hong, S.-H., Lkhambjav, J., Jin, H.-G., & Baik, J.-J. (2023). Spatiotemporal variations of 100 m wind in Mongolia and implications for wind energy resources. *International Journal of Climatology*, 43(7), 3433–3452. <https://doi.org/10.1002/joc.8037>